Sub-GHz Resonant Magnetoelastic Coupling in Epitaxial Fe Thin Films

J.-y S Duquesne, Pauline Rovillain, C. Hepburn, M. Eddrief, P Atkinson, A. Anane, R Ranchal, M. Marangolo

Sub-GHz Resonant Magnetoelastic Coupling in Epitaxial Fe Thin Films

J.-Y. Duquesne,[1, *] P. Rovillain,[1] C. Hepburn,[1] M. Eddrief,[1]
P. Atkinson,[1] A. Anane,[2] R. Ranchal,[3] and M. Marangolo[1]

[1] *Sorbonne Université, CNRS, Institut des NanoSciences de Paris, INSP, UMR7588, F-75005 Paris, France*
[2] *Unité Mixte de Physique CNRS, Thales, Université Paris-Saclay, F-91767 Palaiseau, France*
[3] *Dpt. Fisica de Materiales. Fac. CC. Fisicas. Universidad*
Complutense de Madrid. Ciudad Universitaria s/n, Madrid 28040, Spain

The resonant interaction of surface acoustic waves and spin waves is a potential new tool to handle information. However, the natural precession frequencies of most ferromagnetic materials lie in the 10 GHz range, i.e. far above present common technology for surface acoustic waves. This feature restricts the range of materials of interest. To expand this range, we present here measurements of the acoustic attenuation and velocity, at room temperature, in epitaxial Fe on GaAs(001). Resonant coupling is observed in the sub-GHz regime by proper selection of the orientation and intensity of the applied magnetic field. With a very simple magnetization dynamics model that takes into account the softening of the magnetic precession modes, we are able to describe the observed salient features.

I. INTRODUCTION

The physics of resonant coupling between strain and magnetization, pioneered theoretically by Akhiezer [1] and Kittel [2] and experimentally by Bömmel, Dransfeld [3] and Pomerantz [4] many years ago, experiences today a sustained revival. The crossing of phonon and magnon (or spin wave) branches in the $(\mathbf{k}, \omega)$-space either at magnetic remanence or when a moderate magnetic field is applied to a ferromagnetic material (FM) leads to modes hybridization engendered by magnetoelastic coupling (MEC). The phonons can be thermal lattice vibrations or sound waves excited by transducers. In the former case, the most exciting results concern the so-called spin-Seebeck effect, where spin currents flow in a FM sample due to a thermal gradient [5, 6]. In the latter case, the magnetization precession can be modified by surface acoustic waves (SAWs) in spintronic and magnonic devices. In particular, MEC effects in the sub-GHz regime have allowed SAW induced ferromagnetic resonance (SAW-FMR) to be observed in Ni [7], (Ga,Mn)(As,P) [8] and (Ga,Mn)(As) [9] thin films. Indeed, resonant MEC is so efficient that spin pumping effects could be generated in Co/Pt bilayer at 1.5 GHz [10], and magnetization of (Ga,Mn)(As,P) or (Ga,Mn)(As) thin films could be irreversibly switched [11, 12]. The main advantage of this strain-mediated approach, based on the SAW mature technology, is that phonons can be excited remotely and trigger local magnetization dynamics once they interact with FM materials. This can be done with minimal energy dissipation, very high tunability [13] and high directionality [14].

However, most ferromagnetic materials have precession frequencies well above 5 GHz, i.e. above the highest frequency easily reached by today's SAW technologies. Moreover, their precession frequency increases dramatically with magnetic anisotropy K and saturation magnetization M_s, limiting the ability of research in the field of SAW-FMR. As reported in Fig.1(a) (see the green dashed line) the precession frequency, ν_0, calculated using the Smit and Beljer approach [15] in the emblematic case of Fe thin film, a very important system for spintronic and magnonic applications, is already 10 GHz at zero field. It turns out that ν_0 increases with increasing $M_s B_{ext}$ when an external field $\mathbf{B}_{ext}$ is applied along the easy axis [100]. Such high frequencies restrict the research on SAW-FMR to low magnetization and/or low magnetic anisotropy materials, such as (Ga,Mn)As or (GaMn)(As,P) [8, 9, 11, 12], Ni [3, 7, 10, 14, 16–18], and YIG [19, 20]. Additional requirements for materials for future SAW-based spintronic or magnonic devices is room temperature SAW-FMR, relatively high magnetization for easy detection, a significant magnetoelastic coupling and a low Gilbert damping coefficient α. Here, we show that thin films of Fe epitaxially grown on GaAs(001), a spintronic and magnonic compatible [21] magnetoelastic and piezoelectric heterostucture, give the opportunity to bridge the material gap and to obtain SAW-FMR, at room temperature, below 1 GHz despite the high Fe magnetization ($M_s \simeq 1.7 \times 10^6$ A.m^{-1}), namely around 3 and 40 times larger than in Ni and (Ga,Mn)(As), respectively. Moreover, we show that the resonance is obtained when the field is applied in a very tiny angular range ($\pm 0.1°$), with respect to the magnetic hard axis. The method to lower ν_0 below the GHz regime consists in applying $\mathbf{B}_{ext}$ along the in-plane hard axis of Fe, namely [110] and [1$\bar{1}$0] directions. This strategy of using an applied $\mathbf{B}_{ext}$ was used previously in GaMnAsP [8] and probably in polycrystalline Co at 1.5 GHz [10].

In this configuration, the Smit and Beljer approach predicts a softening of the effective magnetic stiffness, at the saturation field ($B_s \simeq 55$ mT, see experimental magnetization in Fig.1(b)). As shown in the inset of Fig.1(a), at B_s, the precession frequency ν_0 decreases to a value close to the typical SAW frequencies, permitting resonant MEC [22]. Readers interested in the full calculation can find details in Ref.[23]. Such a softening is extremely
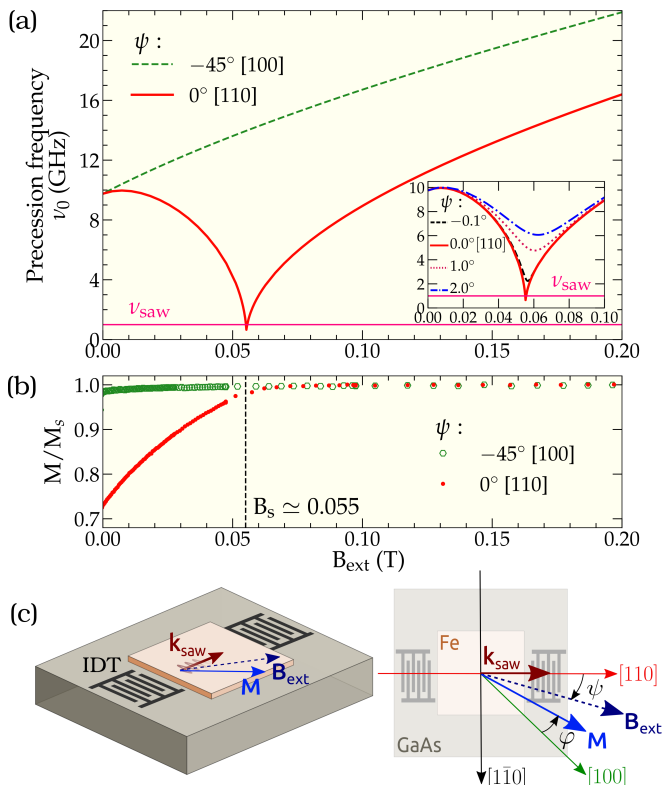

FIG. 1. (a) Calculated precession frequencies in a thin Fe layer (in-plane magnetization) versus applied field amplitude. Field is applied either along easy axis [100] ($\psi = -45°$) or along hard axis [110] ($\psi = 0°$). The effect of the magneto-elastic coupling is to increase the minimum value of ν_0. Inset: Calculated precession frequencies for various small applied field angles ψ with respect to [110]. Calculation parameters are $M_s = 1.7 \times 10^6$ A.m^{-1}, cubic anisotropy $K = 4.7 \times 10^4$ J.m^{-3}, $B_2 = -7 \times 10^6$ J.m^{-3} [24], $C_{11} = 230$ GPa, $C_{12} = 134$ GPa, $C_{44} = 116$ GPa. (b) Measured magnetization along the [100] and [110] axis, by Vibrating Sample Magnetometer, at room temperature. (c) Sketch of the sample.

angular dependent as shown in the inset of Fig.1(a): ν_0 increases dramatically when the magnetic field direction is only 1° off the [110] or the [1$\bar{1}$0] directions. For this reason highly oriented Fe crystals are required to get resonant MEC.

II. EXPERIMENTAL SETUP

In order to obtain high quality and well oriented samples, Fe thin films were grown by molecular beam epitaxy (MBE) on GaAs(001) substrates (undoped). Fe thin films were deposited on a $c(2 \times 2)$ Zn-terminated ZnSe epilayer at 180 °C, grown on a GaAs substrate covered by a thin GaAs buffer, a prototype of a low reactive iron/semiconductor interface [25]. The thickness of the Fe layer is 67 nm. The samples were covered by a protective 10 nm gold capping layer. Fe thin films present the expected epitax-

ial growth conditions, i.e. $[100]_{Fe}//[100]_{ZnSe}//[100]_{GaAs}$ and $(001)_{Fe}//(001)_{ZnSe}//(001)_{GaAs}$ and biaxial magnetic anisotropy, as reported in previous works [25]. A 4×4 mm^2 mesa is then defined by ion etching.

Figure 1(c) represents a sketch of the device under test. We adopted an all electrical excitation/detection of SAWs via the piezoelectric effect in the semi-insulating GaAs substrate, using interdigital transducers (IDTs) [26]. The emitter IDT orientation is such that the acoustic wave vector $\mathbf{k}_{saw}$ is parallel to [110], the most favorable direction for SAW excitation. The split 44 design [27] is used to excite SAW at four harmonic frequencies $n\nu$ where $\nu = 119$ MHz and $n = 1, 3, 5, 7$. Pulsed excitation is used with 500 ns duration. An identical IDT acts as a detector. $\mathbf{k}_{saw}$ direction can be reversed by connecting the input signal to one IDT or to the other. The sample is first subjected to a large external reference field $\mathbf{B}_{ext}$, the magnitude of which is $B_{ref} = 0.4$ T, saturating the sample in the field direction. Then, the field intensity is decreased down to zero, while measuring the amplitude and phase of the acoustic signal. We deduce the relative change in SAW phase velocity, $\Delta V/V = (V(B_{ext}) - V(B_{ref}))/V(B_{ref})$, and the change in SAW attenuation $\Delta\Gamma = \Gamma(B_{ext}) - \Gamma(B_{ref})$ as a function of the field amplitude B_{ext}, at a given field direction ψ and at a given acoustic frequency ν_{saw}. We recall that the acoustic attenuation Γ, in dB per unit length (cm), is $\Gamma = (20/\ln 10)L^{-1}$ where L characterizes the exponential decay $\exp(-x/L)$ of the acoustic wave amplitude versus propagation distance x. All experiments are performed at room temperature.

III. RESULTS

Figures 2 and 3 display our main results. Figure 2 shows the highly directional acoustic properties at 833 MHz. We observe attenuation peaks with a maximum amplitude when $\mathbf{B}_{ext}$ is parallel, within the experimental accuracy of $\pm 1°$, to the in-plane hard axis [110] ($\psi = 0°$). The variation is rather large (5 dB.cm^{-1}) and maximum attenuation is obtained for 0.055 T, which corresponds to the saturation field (Fig.1(b)) and to the minimum of the magnetization precession frequency (Fig.1(a)). The very strong angular dependence of the effect is a striking result: rotating the field from 0.0° to 0.1° divides the attenuation peak by a factor of five. Consequently, the experiments require a 0.05° experimental resolution, at least. It can also be noted that the magnitude of the attenuation peak depends on whether the acoustic wave vector $\mathbf{k}_{saw}$ is parallel or anti-parallel to the applied field $\mathbf{B}_{ext}$, as shown in the inset of Fig.2. Such non-reciprocity effects are well known and are frequently observed in magnetic systems [28–30]. In the following we will only consider the anti-parallel configuration, where the attenuation peak is slightly larger.

In order to put into evidence the effect of the SAW-FMR on the experimental curves, we compare in Fig.3
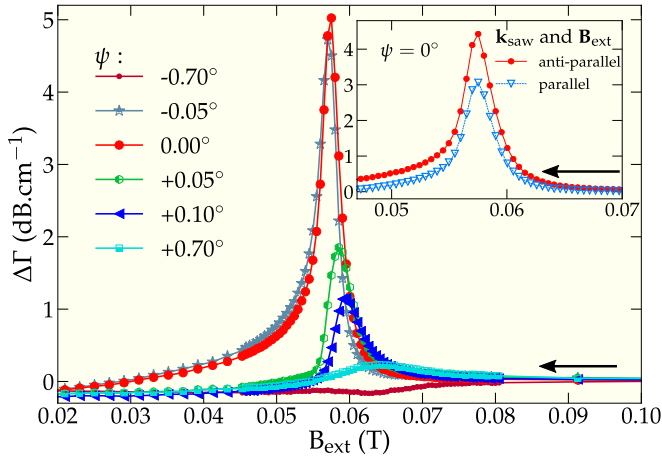
FIG. 2. Variation of acoustic attenuation versus applied magnetic field amplitude B_{ext}. Applied field $\mathbf{B}_{ext}$ is in-plane, at an angle ψ with respect to [110] (hard axis). Field amplitude is decreasing. $\Delta\Gamma = \Gamma(B_{ext}) - \Gamma(B_{ref})$, $B_{ref} = 0.4$ T. Acoustic frequency is 833 MHz. The SAW wavevector $\mathbf{k}_{saw}$ is parallel to [110] direction and anti-parallel to $\mathbf{B}_{ext}$. Inset: same magnetic configuration, $\psi = 0°$. $\mathbf{k}_{saw}$ is either parallel or anti-parallel to $\mathbf{B}_{ext}$.
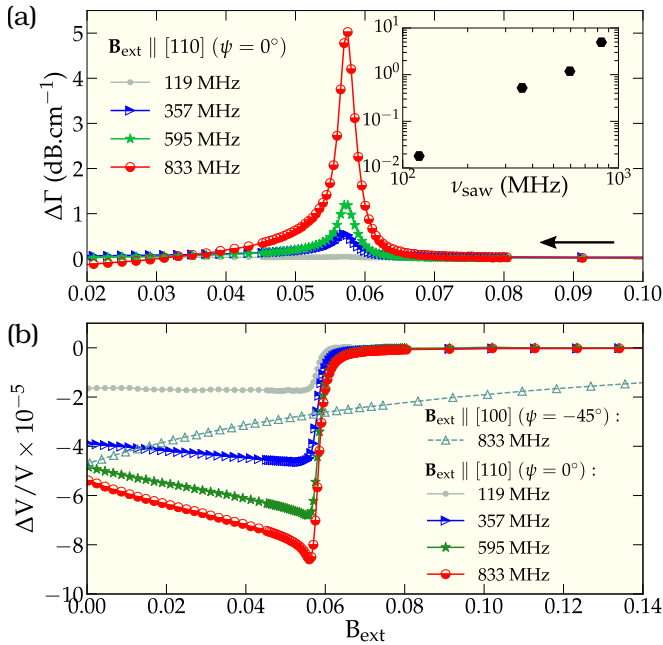

FIG. 3. Variation of acoustic attenuation Γ and velocity V versus applied magnetic field amplitude B_{ext}. Field $\mathbf{B}_{ext}$ is applied in-plane, parallel to [110] (hard axis, $\psi = 0°$), or to [100] (easy axis, $\psi = -45°$). Field amplitude is decreasing. Acoustic frequencies range from 119 MHz to 833 MHz. $\mathbf{k}_{saw}$ is parallel to [110]. At $\psi = 0°$, $\mathbf{k}_{saw}$ and $\mathbf{B}_{ext}$ are anti-parallel. (a) $\Delta\Gamma = \Gamma(B_{ext}) - \Gamma(B_{ref})$, $B_{ref} = 0.4$ T. Inset: Magnitude of the attenuation peak versus frequency ($\psi = 0°$). (b) $\Delta V/V = (V(B_{ext}) - V(B_{ref})/V(B_{ref})$, $B_{ref} = 0.4$ T.
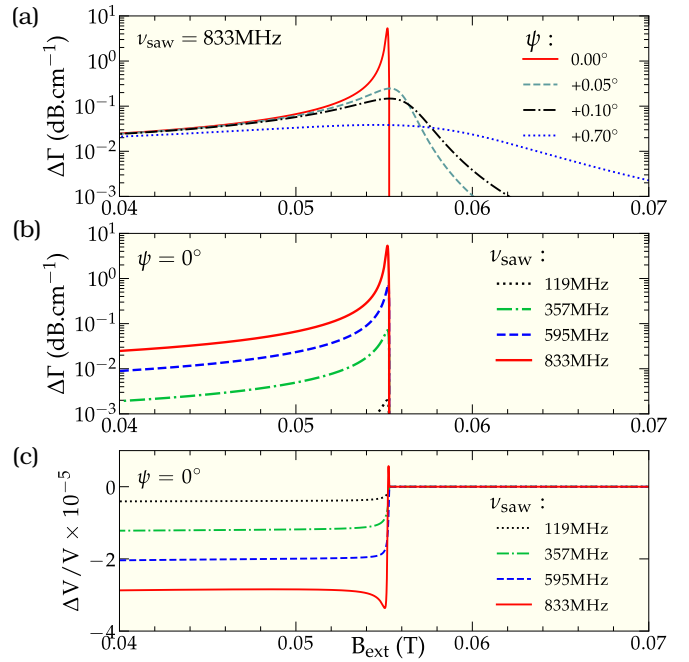

FIG. 4. Computed acoustic attenuation and velocity versus amplitude of the applied field. Field $\mathbf{B}_{ext}$ is applied in the (001) plane, at an angle ψ from [110] (hard axis). Field amplitude is decreasing. (a) Attenuation at various small angles ψ off [110], at 833 MHz. (b) Attenuation at several acoustic frequencies, from 119 MHz to 833 MHz, at $\psi = 0°$. (c) Velocity relative variations at several acoustic frequencies, from 119 MHz to 833 MHz, at $\psi = 0°$. Calculation parameters in (a), (b) and (c) are identical to those in Fig.1(a) and $\alpha = 0.005$.

both SAW attenuation $\Delta\Gamma$ and phase velocity variations $\Delta V/V$ at several acoustic frequencies ν_{saw} and for two magnetic field directions. Let us first consider $\mathbf{B}_{ext}$ parallel to the in-plane hard axis [110] ($\psi = 0°$). At high external field, both SAW attenuation and velocity are constant, indicating that there is no coupling between SAW and magnetization. Below 0.08 T, we observe velocity and attenuation variations indicating an effective magneto-elastic coupling with a maximum close to the saturation field B_s. In the inset we show that the magnitude of the attenuation peak is roughly proportional to ν_{saw}^3. Moreover, the velocity depends on the frequency and also on small angular variation around this configuration (not shown here). It is also worthwhile to notice the kink in the velocity variations at 833 MHz around 0.055 T which fades away when the frequency decreases. A totally different behavior is observed when the field is applied along [100] ($\psi = -45°$). The attenuation is constant (not shown) and the velocity changes smoothly up to high fields (see Fig.3(b)).

IV. PHENOMENOLOGICAL MODEL

In order to evaluate how resonant MEC affects the field dependence of velocity and attenuation, we study magnetization dynamics in the framework of Landau-Lifshitz-Gilbert (LLG) equations.

$$\frac{d\mathbf{m}}{dt} = -\gamma\,\mathbf{m}\times\mathbf{B}_{eff} + \alpha\,\mathbf{m}\times\frac{d\mathbf{m}}{dt} \quad ; \quad \mathbf{B}_{eff} = -\nabla_{\mathbf{m}} f \quad (1)$$

where $\mathbf{m}$ is the normalized magnetization $\mathbf{M}/M_s$. γ is the absolute value of the gyromagnetic factor, α is the Gilbert damping coefficient. f is the normalized free energy F/M_s of the layer. The free energy F is the sum $F = F_z + F_d + F_{mc} + F_{mec} + F_{el}$, where the various terms are the Zeeman, the demagnetizing, the magnetocrystalline anisotropy, the magnetoelastic and the elastic energy terms. The relative weights of each terms depends on the intensity and the direction of the external magnetic field (see for example [23]). The magneto-elastic free energy of a cubic solid reads :

$$\begin{aligned} F_{mec} = \ & B_1\left[\varepsilon_{xx}(m_x^2-\tfrac{1}{3}) + \varepsilon_{yy}(m_y^2-\tfrac{1}{3}) + \varepsilon_{zz}(m_z^2-\tfrac{1}{3})\right] \\ & + 2B_2\left[\varepsilon_{xy}m_xm_y + \varepsilon_{xz}m_xm_z + \varepsilon_{yz}m_ym_z\right] \end{aligned}$$
$$(2)$$

B_1 and B_2 are phenomenological coupling constants [31]. ε_{ij} are the strain components, expressed in the standard cubic frame. For small deviations from equilibrium, the LLG equation can be linearized [23, 32]:

$$\begin{cases} \dfrac{d\delta\varphi}{dt} = \kappa_1\,\delta\theta + \kappa_2\,\delta\varphi + \displaystyle\sum_{i\leq j}\kappa_{ij}\,\delta\varepsilon_{ij} \\[2mm] \dfrac{d\delta\theta}{dt} = \zeta_1\,\delta\theta + \zeta_2\,\delta\varphi + \displaystyle\sum_{i\leq j}\zeta_{ij}\,\delta\varepsilon_{ij} \end{cases} \quad (3)$$

θ and φ are the magnetization $\mathbf{M}$ polar and azimuthal angles (with respect to [001] and [100], respectively). The κ and ζ terms are related to the second order derivatives $f_{\theta,\theta}$, $f_{\varphi,\varphi}$ and $f_{\theta,\varphi}$ of the normalized free energy (for details, see [23]). In our experiments, the deviations $\delta\varepsilon_{ij}$ are due to the surface acoustic wave. *To simplify the calculations, we crudely assume that a bulk longitudinal wave, propagating along* [110] *may catch the physics of the interaction between the acoustic wave and* $\mathbf{M}$. Such a simple model has already been used [33]. More sophisticated calculations would improve certainly the agreeement with the experimental data but at the expense of complexity [34–36]. Then, the displacement field $\mathbf{u}$ and precession angles variations $\delta\varphi$ and $\delta\theta$ read:

$$\begin{cases} u_1' = U\exp(i(\omega t - kx')) \\ u_2' = u_3' = 0 \\ \delta\varphi = \Phi\exp(i(\omega t - kx')) \\ \delta\theta = \Theta\exp(i(\omega t - kx')) \end{cases} \quad (4)$$

(here, and in the following, any component expressed in the rotated frame ([110], [$\bar{1}$10], [001]) will be primed). From Eqs.(3) and (4), we derive:

$$\delta\varphi = \frac{-ik}{2}\frac{(i\omega-\zeta_1)\kappa_{12}+\zeta_{12}\kappa_1}{(i\omega-\kappa_2)(i\omega-\zeta_1)-\kappa_1\zeta_2}u_1' \quad (5)$$

The acoustic wave dynamics is governed by the Newton equation. In our case:

$$\rho\,\frac{\partial^2 u_1'}{\partial t^2} = \frac{\partial \sigma_{11}'}{\partial x'} \quad (6)$$

where ρ is the mass density of the magnetic layer and the strain $\sigma_{11}' = \frac{\partial F}{\partial\varepsilon_{11}'}$ is derived from the magnetic free energy F:

$$\sigma_{11}' = C_{11}'\delta\varepsilon_{11}' + B_2\cos 2\bar{\varphi}\,\delta\varphi \quad (7)$$

$\bar{\varphi}$ is the equilibrium value of the azimuthal angle φ. The relation between $\bar{\varphi}$ and ψ can be derived in a Stoner and Wohlfarth approach, by minimizing the free energy. At saturation, ψ and $\bar{\varphi}$ are linked by $\psi = \bar{\varphi} - \pi/4$. C_{11}' is the C_{11} elastic constant of the Fe layer, in the rotated frame ([110], [$\bar{1}$10], [001]). The magnetoelastic term in Eq.7 reflects the maximum torque, exerted by the SAW on the magnetization, for $\bar{\varphi} = 0°$ or $90°$. From equations 5, 6 and 7, we derive:

$$\rho\,\omega^2 = \widetilde{C_{11}'}\,k^2 \quad (8)$$

where:

$$\widetilde{C_{11}'} = C_{11}' + \frac{B_2^2\gamma}{M_s}\cos^2(2\bar{\varphi})\frac{(\omega^2-\omega_0^2)\,\gamma f_{\theta,\theta} - 2\alpha\omega^2\tau^{-1} + i\left[2\omega\tau^{-1}\gamma f_{\theta,\theta} + \alpha\omega\left(\omega^2-\omega_0^2\right)\right]}{\left(\omega^2-\omega_0^2\right)^2 + 4\omega^2\tau^{-2}} \quad (9)$$

τ is the relaxation time and $\omega_0 = 2\pi\nu_0$ is the magnetization precession resonant radial frequency also defined in [23] as:

$$\tau^{-1} = \frac{1}{2}\frac{\alpha\gamma}{1+\alpha^2}(f_{\theta,\theta} + f_{\varphi,\varphi}) \quad (10)$$

$$\omega_0 = \gamma\sqrt{f_{\theta,\theta}f_{\varphi,\varphi}} \quad (11)$$

$\widetilde{C_{11}'}$ is an effective elastic modulus governing the propagation of a bulk longitudinal wave along [110], in an infinite medium with elastic and magnetic properties of the layer. We take into account the finite thickness d of the thin film by an effective medium approach. The penetration depth of a SAW is roughly equal to its wavelength λ. Then, we assume that the relevant effective

modulus, governing the propagation of the SAW, is the average of the layer and substrate modulus, weighted by d and $(\lambda - d)$, respectively:

$$C' = \frac{d \, \widetilde{C'_{11}} + (\lambda - d)C'_s}{\lambda} \qquad (12)$$

C'_s is the C_{11} elastic modulus of the substrate, in the rotated frame. The velocity v and acoustic decay length L are related to the real and imaginary parts of C' [37]:

$$\frac{\Delta v}{v} = \frac{d}{2\lambda} \frac{\Delta \Re(\widetilde{C'_{11}})}{C'_s} \quad ; \quad L^{-1} = \frac{\omega^2 d}{4\pi v^2} \frac{\Im(\widetilde{C'_{11}})}{C'_s} \qquad (13)$$

We show now that this simple model catches the physics of the observed phenomena, i.e. a highly directional resonant process. As discussed above, magnetoelastic resonance can be achieved close to B_s, as shown in the inset of Fig1(a). A careful inspection of Eqs. (9) and (13) reveals the resonant character of $\widetilde{C'_{11}}$ modulus with a maximum when ω_0 and ω_{saw} match, leading to maximum attenuation and velocity variations. This is visible in Fig.4(a) which shows the calculated attenuation for several small angles ψ with respect to [110], at 833 MHz.

It should be noted that our simple model predicts attenuation peaks exhibiting a strong dependance on ψ, in agreement with the experiments. This is related to the sensitivity of the frequency matching condition with respect to ψ (see inset of Fig.1(a)). Figure 4(b) also displays the attenuation at various frequencies, at $\psi = 0°$. At 833 MHz, the attenuation is much larger than at lower frequencies, due to the matching condition $\omega_{saw} = \omega_0$. The magnitude of the calculated peak is close to the experimental value (5 dB.cm^{-1}) and decreases drastically at lower frequencies. The experimental curves are wider than the theoretical ones. We ascribe this observation to the mosaicity of the sample (FWHM of the (002) planes $\simeq 0.3°$, measured by X Ray diffraction), responsible for a spreading of the resonance frequencies at a given $\mathbf{B}_{ext}$. At low frequencies, the calculation underestimates the coupling since the measured attenuation is slightly larger than the one predicted by our simple model. Concerning the sound velocity, our calculation gives the correct order of magnitude and describes the trend of the magnetic field dependence as reported in Fig.4(c). A sharp variation is observed at all frequencies for $B_{ext} = B_s$. At 833 MHz, we notice that the variation is maximum and it is characterized by two kinks just above and below the sharp step. The wider kink well reproduces the one observed in experiments at 833 MHz (Fig.3(b)), indicating that the condition $\omega_{saw} = \omega_0$ is fullfilled. This point is expected from the analysis of Eq.(9). The narrower kink is not observed experimentally because of a convolution effect due to the mosaicity of the sample (not shown).

Finally, the $\omega_{saw} = \omega_0$ condition is certainly fulfilled even at 595 MHz since we observe a small kink below the sharp step at 595 MHz (see Fig.3(b)).

V. CONCLUSION

Our experimental findings prove that resonant phonon-magnon coupling is comfortably obtained in epitaxial Fe thin films on piezoelectric GaAs(001), even in the sub-GHz regime. Magnetization dynamics can be switched on/off by a slight variation of the magnetic field direction. Inevitably, resonant magneto-elastic coupling leads to magnetization dynamics triggering and to modifications of the spin waves amplitude and phase, paving the way to a remote control of spin wave propagation via acoustic waves that are characterized by millimeters decay length. Consequently, SAWs might be a valuable tool for spin wave and spin currents excitation and spin wave manipulation (dephasing, amplitude modulation and even gap opening) in common FM materials, like bcc Fe, $Fe_{1-x}Ga_x$ and Py, characterized by magnetocrystalline or induced magnetic anisotropy [38].

[1] A. Akhiezer, V. Bariakhtar, and S. Peletminskii, Coupled magnetoelastic waves in ferromagnetic media and ferroacoustic resonance, Soviet Physics JETP-USSR **8**, 157 (1959).

[2] C. Kittel, Interaction of spin waves and ultrasonic waves in ferromagnetic crystals, Phys. Rev. **110**, 836 (1958).

[3] H. Bömmel and K. Dransfeld, Excitation of hypersonic waves by ferromagnetic resonance, Phys. Rev. Lett. **3**, 83 (1959).

[4] M. Pomerantz, Excitation of spin-wave resonance by microwave phonons, Phys. Rev. Lett. **7**, 312 (1961).

[5] T. Kikkawa, K. Shen, B. Flebus, R. A. Duine, K.-i. Uchida, Z. Qiu, G. E. W. Bauer, and E. Saitoh, Magnon polarons in the spin seebeck effect, Phys. Rev. Lett. **117**, 207203 (2016).

[6] B. Flebus, K. Shen, T. Kikkawa, K.-i. Uchida, Z. Qiu, E. Saitoh, R. A. Duine, and G. E. W. Bauer, Magnon-polaron transport in magnetic insulators, Phys. Rev. B

95, 144420 (2017).

[7] M. Weiler, L. Dreher, C. Heeg, H. Huebl, R. Gross, M. S. Brandt, and S. T. B. Goennenwein, Elastically driven ferromagnetic resonance in nickel thin films, Phys. Rev. Lett. **106**, 117601 (2011).

[8] L. Thevenard, C. Gourdon, J. Y. Prieur, H. J. von Bardeleben, S. Vincent, L. Becerra, L. Largeau, and J.-Y. Duquesne, Surface-acoustic-wave-driven ferromagnetic resonance in (Ga,Mn)(As,P) epilayers, Phys. Rev. B **90**, 094401 (2014).

[9] P. Kuszewski, J.-Y. Duquesne, L. Becerra, A. Lemaître, S. Vincent, S. Majrab, F. Margaillan, C. Gourdon, and L. Thevenard, Optical probing of rayleigh wave driven magnetoacoustic resonance, Phys. Rev. Applied **10**, 034036 (2018).

[10] M. Weiler, H. Huebl, F. S. Goerg, F. D. Czeschka, R. Gross, and S. T. B. Goennenwein, Spin pumping with coherent elastic waves, Phys. Rev. Lett. **108**, 176601 (2012).

[11] L. Thevenard, I. S. Camara, S. Majrab, M. Bernard, P. Rovillain, A. Lemaître, C. Gourdon, and J.-Y. Duquesne, Precessional magnetization switching by a surface acoustic wave, Phys. Rev. B **93**, 134430 (2016).

[12] P. Kuszewski, I. Camara, N. Biarrotte, L. Becerra, J. von Bardeleben, W. Savero Torres, A. Lemaître, C. Gourdon, J.-Y. Duquesne, and L. Thevenard, Resonant magneto-acoustic switching: influence of rayleigh wave frequency and wavevector, Journal of Physics: Condensed Matter **30**, 244003 (2018).

[13] D. Labanowski, A. Jung, and S. Salahuddin, Power absorption in acoustically driven ferromagnetic resonance, Applied Physics Letters **108**, 022905 (2016), https://doi.org/10.1063/1.4939914.

[14] P. G. Gowtham, T. Moriyama, D. C. Ralph, and R. A. Buhrman, Traveling surface spin-wave resonance spectroscopy using surface acoustic waves, Journal of Applied Physics **118**, 233910 (2015), https://doi.org/10.1063/1.4938390.

[15] J. Smit and G. Beljers, Ferromagnetic resonance absorption in $BaFe_{12}O_{19}$, a highly anisotropic crystal, Philips Res. Rep. **10**, 113 (1955).

[16] I. Feng, M. Tachiki, C. Krischer, and M. Levy, Mechanism for the interaction of surface waves with 200 nickel films, Journal of Applied Physics **53**, 177 (1982), https://doi.org/10.1063/1.331582.

[17] X. Li, D. Labanowski, S. Salahuddin, and C. S. Lynch, Spin wave generation by surface acoustic waves, Journal of Applied Physics **122**, 043904 (2017), https://doi.org/10.1063/1.4996102.

[18] Y. Nozaki and S. Yanagisawa, Excitation of ferromagnetic resonance using surface acoustic waves, Electrical Engineering in Japan **204**, 3 (2018), https://onlinelibrary.wiley.com/doi/pdf/10.1002/eej.23099.

[19] A. Kamra, H. Keshtgar, P. Yan, and G. E. W. Bauer, Coherent elastic excitation of spin waves, Phys. Rev. B **91**, 104409 (2015).

[20] J. Holanda, D. S. Maior, A. Azevedo, and S. M. Rezende, Detecting the phonon spin in magnonphonon conversion experiments, Nature Physics **14**, 500 (2018).

[21] O. Gladii, D. Halley, Y. Henry, and M. Bailleul, Spin-wave propagation and spin-polarized electron transport in single-crystal iron films, Phys. Rev. B **96**, 174420 (2017).

[22] It is worthwhile to notice that such low frequencies are not probed by Brillouin Light Scattering (BLS) experiments, usually employed to measure the magnetic field dependance of magnetization dynamics, i.e. the minimum is smeared out by BLS, hiding the possibility to get sub-GHz resonant MEC.

[23] J.-Y. Duquesne, C. Hepburn, P. Rovillain, and M. Marangolo, Magnetocrystalline and magnetoelastic constants determined by magnetization dynamics under static strain, Journal of Physics: Condensed Matter **30**, 394002 (2018).

[24] M. Barturen, *Anisotropie magnétique et couplage magnéto-élastique dans des couches minces de FeGa épitaxié sur GaAs(001)*, Ph.D. thesis, P. and M. Curie University (France) (2014).

[25] M. Marangolo, F. Gustavsson, G. M. Guichar, M. Eddrief, J. Varalda, V. H. Etgens, M. Rivoire, F. Gendron, H. Magnan, D. H. Mosca, and J.-M. George, Structural and magnetic anisotropies of FeZnSe(001) thin films, Phys. Rev. B **70**, 134404 (2004).

[26] D. Royer and E. Dieulesaint, *Elastic Waves in Solids II*, Advanced Texts in Physics (Springer-Verlag Berlin Heidelberg, 2000).

[27] F. J. R. Schülein, E. Zallo, P. Atkinson, O. G. Schmidt, R. Trotta, A. Rastelli, A. Wixforth, and H. J. Krenner, Fourier synthesis of radiofrequency nanomechanical pulses with different shapes, Nature Nanotechnology **10**, 512 (2015).

[28] M. F. Lewis and E. Patterson, Acoustic surface wave isolator, Applied Physics Letters **20**, 276 (1972), https://doi.org/10.1063/1.1654147.

[29] R. Camley, Nonreciprocal surface waves, Surface Science Reports **7**, 103 (1987).

[30] R. Sasaki, Y. Nii, Y. Iguchi, and Y. Onose, Nonreciprocal propagation of surface acoustic wave in $Ni/LiNbO_3$, Phys. Rev. B **95**, 020407 (2017).

[31] We use here $2B_2$ rather than B_2 (in [23]) to conform with usage [2].

[32] T. L. Linnik, A. V. Scherbakov, D. R. Yakovlev, X. Liu, J. K. Furdyna, and M. Bayer, Theory of magnetization precession induced by a picosecond strain pulse in ferromagnetic semiconductor (Ga,Mn)As, Phys. Rev. B **84**, 214432 (2011).

[33] L. Dreher, M. Weiler, M. Pernpeintner, H. Huebl, R. Gross, M. S. Brandt, and S. T. B. Goennenwein, Surface acoustic wave driven ferromagnetic resonance in nickel thin films: Theory and experiment, Phys. Rev. B **86**, 134415 (2012).

[34] A. K. Ganguly, K. L. Davis, and D. C. Webb, Magnetoelastic surface waves on the (110) plane of highly magnetostrictive cubic crystals, Journal of Applied Physics **49**, 759 (1978), https://doi.org/10.1063/1.324655.

[35] H. Zhou, A. Talbi, N. Tiercelin, and O. Bou Matar, Multilayer magnetostrictive structure based surface acoustic wave devices, Applied Physics Letters **104**, 114101 (2014), https://doi.org/10.1063/1.4868530.

[36] P. G. Gowtham, D. Labanowski, and S. Salahuddin, Mechanical back-action of a spin-wave resonance in a magnetoelastic thin film on a surface acoustic wave, Phys. Rev. B **94**, 014436 (2016).

[37] A. S. Nowick and B. S. Berry, *Anelastic relaxation in crystalline solids* (Academic Press, 1972).

[38] A. Muñoz-Noval, A. Ordóñez-Fontes, and R. Ranchal, Influence of the sputtering flow regime on the structural

properties and magnetic behavior of Fe-Ga thin films (Ga∼30 at.%), Phys. Rev. B **93**, 214408 (2016).